The Astronomical Journal, 150:152 (10pp), 2015 November doi:10.1088/0004-6256/150/5/152

PHYSICAL OBSERVATIONS OF (196256) 2003 EH1, PRESUMED PARENT OF THE QUADRANTID METEOROID STREAM

Toshihiro Kasuga[1,3] and David Jewitt[2,3]
[1] Planetary Exploration Research Center, Chiba Institute of Technology, 2-17-1 Tsudanuma, Narashino, Chiba 275-0016, Japan; kasuga@perc.it-chiba.ac.jp
[2] Department of Earth, Planetary and Space Sciences and Department of Physics and Astronomy, University of California at Los Angeles, 595 Charles Young Drive East, Los Angeles, CA 90095-1567, USA
Received 2015 July 14; accepted 2015 September 3; published 2015 October 21

ABSTRACT

The near-Earth asteroid (196256) 2003 EH1 has been suggested to have a dynamical association with the Quadrantid meteoroid stream. We present photometric observations taken to investigate the physical character of this body and to explore its possible relation to the stream. We find no evidence for ongoing mass loss. A model fitted to the point-like surface brightness profile at 2.1 AU limits the fractional contribution to the integrated brightness by the near-nucleus coma to $\leqslant$2.5%. Assuming an albedo equal to those typical of cometary nuclei ($p_{\mathrm{R}} = 0.04$), we find that the effective nucleus radius is $r_{\mathrm{e}} = 2.0 \pm 0.2$ km. Time-resolved *R*-band photometry can be fitted by a two-peaked light curve having a rotational period of 12.650 ± 0.033 hr. The range of the light curve, $\Delta m_{\mathrm{R}} = 0.44 \pm 0.01$ mag, is indicative of an elongated shape having an axis ratio of $\sim$1.5 projected into the plane of the sky. The asteroid shows colors slightly redder than the Sun, being comparable with those of C-type asteroids. The limit to the mass loss rate set by the absence of the resolved coma is $\lesssim 2.5 \times 10^{-2}$ kg s^{-1}, corresponding to an upper limit on the fraction of the surface that could be sublimating water ice $f_A \lesssim 10^{-4}$. Even if sustained over the 200–500 year dynamical age of the Quadrantid stream, the total mass loss from 2003 EH1 would be too small to supply the reported stream mass (10^{13} kg), implying either that the stream has another parent or that mass loss from 2003 EH1 is episodic.

Key words: comets: general – meteorites, meteors, meteoroids – minor planets, asteroids: general

1. INTRODUCTION

The near-Earth asteroid (196256) 2003 EH1 (hereafter 2003 EH1) was discovered on UT 2003 March 6 in the course of the Lowell Observatory Near-Earth-Object Search (Skiff 2003). Dynamical studies show that the asteroid is associated with, and is presumed to be the parent body of, the Quadrantid meteoroid stream (Jenniskens 2004; Williams et al. 2004; Wiegert & Brown 2005; Babadzhanov et al. 2008; Jopek 2011; Abedin et al. 2015). The orbit has a semimajor axis $a = 3.126$ AU, eccentricity $e = 0.619$, and inclination $i = 70\overset{\circ}{.}8$ (NASA/JPL HORIZON). The Tisserand parameter with respect to Jupiter, $T_{\mathrm{J}} = 2.063$, is consistent with the dynamical classification of 2003 EH1 as a Jupiter-family comet (JFC), although no activity has yet been reported. A straightforward interpretation is that 2003 EH1 is a dormant or weakly active comet (Koten et al. 2006; Babadzhanov et al. 2008; Borovička et al. 2010; Tancredi 2014).

Dynamical studies of the recent ($<10^4$ year) evolution of the orbit of 2003 EH1 under the action of planetary perturbations are suggestive in this regard. The semimajor axis lies close to the 2:1 mean-motion resonance with Jupiter at 3.27 AU, causing strong orbital variations that drive 2003 EH1 into a Sun-approaching dynamical state (Wiegert & Brown 2005; Neslušan et al. 2013a; Fernández et al. 2014). Numerical integrations show that the perihelion distance has increased approximately linearly with time from 0.2 AU 1000 years ago to the present-day value of 1.2 AU. The minimum $q \sim 0.12$ AU ($e \sim 0.96$) occurred only $\sim$1500 year ago (Neslušan et al. 2013a; Fernández et al. 2014). As a result, it is reasonable to expect that the surface layers should have been devolatilized at the high temperatures reached at past perihelia, leading to the present, apparently inert state.

The Quadrantid meteor shower was first reported in 1835 (Quetelet 1839). The shower has a very short duration in its core activity (Earth crosses the core stream in $\sim$0.5 day) superimposed on a broader, long-lived background activity (crossing time $\sim$4 days), suggesting that young and old meteoroid streams coexist (Wiegert & Brown 2005 and references therein). The width of a meteor stream increases with age as a result of the progressive influence of planetary perturbations. The small width of the Quadrantid core stream indicates ejection ages of only $\sim$200–500 years (Jenniskens 2004; Williams et al. 2004; Wiegert & Brown 2005; Abedin et al. 2015) and there is some suggestion that the first reports of meteoroid stream activity coincide with the formation of the stream. On the other hand, the broader background stream implies larger ages of perhaps $\sim$3500 years or more (Ohtsuka et al. 1995; Wiegert & Brown 2005; Kanuchová & Neslušan 2007; Ohtsuka et al. 2008). Comet 96P/Machholz is also suspected to form part of the "Quadrantid complex," possibly releasing meteoroids between 2000–5000 years ago (McIntosh 1990; Babadzhanov & Obrubov 1991; Gonczi et al. 1992; Jones & Jones 1993; Wiegert & Brown 2005). Comet 96P/Machholz currently has a small perihelion orbit ($a = 3.034$ AU, $e = 0.959$, $i = 58\overset{\circ}{.}312$ and $q = 0.124$ AU from NASA/JPL HORIZON) substantially different from that of 2003 EH1. Despite these differences, the rapid dynamical evolution shows that it is possible that 2003 EH1 is a split fragment of 96P/Machholz or that both were released from a now defunct precursor body (together defining the Machholz complex: Sekanina & Chodas 2005). One or both of these bodies could be the parents of the Quadrantid

[3] Visiting Astronomer, Kitt Peak National Observatory, National Optical Astronomy Observatory, which is operated by the Association of Universities for Research in Astronomy (AURA) under cooperative agreement with the National Science Foundation.

Table 1
Observation Log

UT Date	Telescope[a]	Integration (s)	Filter[b]	R^c (AU)	Δ^d (AU)	α^e (deg)
2013 Aug 8	KPNO 2.1	180	83 *R*	2.5427	2.1059	22.81
2013 Aug 9	KPNO 2.1	180	1 *B*, 48 *R*	2.5357	2.1033	22.91
		200	2 *B*			
		120	1 *V*			
		140	3 *V*			
2013 Aug 12	KPNO 2.1	200	3 *B*	2.5145	2.0964	23.19
		140	3 *V*			
		180	74 *R*			
		300	3 *I*			
2013 Oct 2	Keck 10	260	1 *R*	2.1390	2.0383	27.59
		100	1 *R*			

Notes.
[a] KPNO 2.1 = Kitt Peak 2.1 m telescope. Keck 10 = 10 m Keck I telescope.
[b] Filter and number of images.
[c] Heliocentric distance.
[d] Geocentric distance.
[e] Phase angle.

meteoroids (Kanuchová & Neslušan 2007; Babadzhanov et al. 2008; Neslušan et al. 2013a, 2013b, 2014).

The small lifetime of the Quadrantid stream suggests that 2003 EH1 could still be active, particularly when in the small perihelion orbital state. In this paper we report the first measurements of the physical properties of 2003 EH1, including colors, limits on coma activity, size, mass loss rate, fractional active area on the object, and rotational period and further discuss the possible relation of this body to the Quadrantid stream and complex.

2. OBSERVATIONS

We observed on the nights of UT 2013 August 8, 9, and 12 using the Kitt Peak National Observatory 2.1 m diameter telescope (hereafter, KPNO 2.1) in Arizona and on October 2 at the Keck I 10 m diameter telescope at the top of Mauna Kea, HI. The KPNO 2.1 employed a STA3 4000 × 2600 pixel charged-coupled device (CCD) camera at the f/7.5 Cassegrain focus. We used a 2 × 2 binned image scale of $0\farcs298$ pixel^{-1}, giving a field of view (FOV) of approximately $9\farcm6 \times 6\farcm7$. On Keck I, the Low Resolution Imaging Spectrometer (LRIS) camera (Oke et al. 1995) was used to image the object. The LRIS camera has two separate channels having red and blue optimized CCD imagers separated by a dichroic filter. One is a red-side detector having a mosaic of two LBNL 2000 × 4000 pixels (Rockosi et al. 2010) and the other is a blue-side detector having a mosaic of two 2K × 4K Marconi CCDs, both with imaging scales of $0\farcs135$ pixel^{-1}. The FOV in both modes of operation is $6\farcm0 \times 7\farcm8$. For imaging data, both telescopes were tracked non-sidereally to follow the motion of 2003 EH1. On KPNO 2.1, images were taken through the Johnson–Kron–Cousins *BVRI* filter system. On Keck I, images in the *R* filter were recorded using the red-side detector of LRIS. The images were flattened by subtracting a bias image and dividing by a bias-subtracted flat-field image constructed using artificial illumination of the inside of each dome for each filter. Photometric calibrations were obtained using standard stars from Landolt (1992), including SA113-163, SA113-337, SA113-265, and SA92-412. The FWHM measured on 2003 EH1 varied from $\sim 0\farcs8$ to $1\farcs5$. The sky was photometric on the nights of UT 2013 August 9, 12, and October 2. Data obtained under slightly non-photometric conditions on August 8 were photometrically calibrated using field stars observed on a photometric night. An observational log is given in Table 1.

3. RESULTS

Object 2003 EH1 appeared point-like in all image data (see Figure 1). Photometry was performed using synthetic circular apertures projected onto the sky. The photometric aperture radius used was twice the FWHM in the image ($\sim 1\farcs6$–$3\farcs0$) and the sky background was determined within a concentric annulus having projected inner and outer radii of $6\farcs6$ and $13\farcs2$, respectively. Photometric results are listed in Tables 2 and 3.

3.1. Colors

The weighted mean colors of 2003 EH1 are $B - V = 0.69 \pm 0.01$, $V - R = 0.39 \pm 0.01$, and $R - I = 0.38 \pm 0.01$ from $N = 16$ measurements (see Table 2). Figures 2 and 3 show $V - R$ versus $B - V$ and $R - I$ versus $V - R$, respectively, together with the Tholen taxonomy classes (Tholen 1984) from Dandy et al. (2003). The $V - R$ data of 2003 EH1 together with the various small body populations and the solar color are summarized in Table 4. We also list the normalized reflectivity slope, S' [%(1000 Å)$^{-1}$], measured in the $V - R$ region (Luu & Jewitt 1990).

The optical colors of 2003 EH1 are similar to, but slightly redder than, those of the Sun (Table 2), being most taxonomically compatible with those of C-type asteroids (Figures 2 and 3). The $V - R$ color (0.39 ± 0.01) is similar to the weighted mean color of 96P/Machholz ($V - R = 0.40 \pm 0.03$ from Licandro et al. 2000 and Meech et al. 2004). Table 4 indicates that 2003 EH1 has a spectral slope less red than those of dead comets, cometary nuclei, Jupiter Trojans, and Damocloids, many of which are spectrally classified as D-type asteroids (Jewitt & Luu 1990; Fitzsimmons et al. 1994; Jewitt 2002, 2004, 2005; Fornasier et al. 2007; Karlsson et al. 2009). On the other hand, 2003 EH1 has a nearly neutral spectral

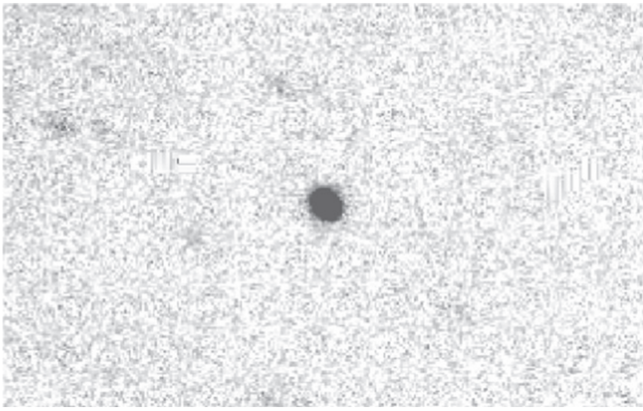

Figure 1. *R*-band image of 2003 EH1 taken by the Keck I 10 m telescope on UT 2013 October 2. The image has a total integration time of 360 s. The frame size is $40'' \times 25''$. No coma or tail is visible on the object, which has an FWHM of $0\overset{''}{.}86$.

slope, as do many main belt comets (MBCs: Hsieh & Jewitt 2006) (see Table 4).

We note that the colors and S' of 2003 EH1 are remarkably less red than the average colors of cometary nuclei (Jewitt 2002; Lamy et al. 2004). This could be a result of past thermal processing when the object had a perihelion far inside Earth's orbit. Indeed, the weighted mean color of eight near-Sun asteroids having perihelion distances $\leqslant$0.25 AU (subsolar temperatures $\geqslant$800 K) is $V - R = 0.36 \pm 0.01$ (Jewitt 2013), consistent with the color of EH1. We conclude that the colors of 2003 EH1 are broadly consistent with those measured in dead cometary nuclei, presumably as a result of mantling from now-gone activity.

3.2. Surface Brightness

Here we search for evidence of a coma, which would indicate ongoing mass loss from 2003 EH1. We compared the measured surface brightness profile with the profiles of a field star nearby and a seeing-convolution model. Since the non-sidereal motion of 2003 EH1 makes the images of background stars appear trailed in the data, the one-dimensional surface brightness profiles were examined using the procedures of Luu & Jewitt (1992). To determine the profile, we used two *R*-band images taken using the Keck I telescope on UT 2013 October 2 (Table 1), without any background contamination. The Keck signal-to-noise ratio, $S/N \geqslant 70$–140, is greater than that of the KPNO 2.1 ($S/N \simeq 20$–30). Each image was rotated to bring the direction of the projected motion of 2003 EH1 to the horizontal, shifted to align the images using fifth-order polynomial interpolation, then combined into a single image (total integration time of 360 s). The resulting image of 2003 EH1 has an FWHM of $0\overset{''}{.}86$, compatible with the seeing in the individual images used to make the composite. The seeing was determined from the point-spread function of a field star measured perpendicular to the direction of the trail and convolved with "nucleus plus coma" comet models. In the model images, each of which is 100×100 pixels, the nucleus was represented as a "point source" located at the central pixel embedded in a circularly symmetric coma of varying activity levels. The surface brightness is assumed to decrease inversely with distance from the nucleus, as expected for steady-state, isotropic expansion of a coma. The principal parameter η, is equal to the ratio of the cross sections of the coma to that of the nucleus, with $\eta = 0$ corresponding to a bare nucleus and $\eta = 1$ to a nucleus and coma having the same cross sections within the projected photometry aperture (Luu & Jewitt 1992). The flux density of each pixel in the coma is given by K/r, where K is a constant of proportionality and r is the distance from the nucleus in the plane of the sky.

Figure 4 shows surface brightness profiles of 2003 EH1, the field star (solid line), and seeing-convolution models with coma levels of $\eta = 0.03$, 0.05, 0.10 (dotted lines). All profiles are normalized to be unity at the center for comparison. The surface brightness profiles of 2003 EH1 and a field star were measured in the direction perpendicular to the motion of the asteroid. The individual profile, after the sky background subtraction, was averaged along the rows over the width of the asteroid and the field star. The normalized profiles of the asteroid and the field star are indistinguishable. From the figure we set an upper limit on the coma level of $\eta \lesssim 0.025 \pm 0.007$.

A limit to the near-nucleus coma can also be set on the basis of simple aperture photometry (Jewitt & Danielson 1984). Observations set a limit to the surface brightness, $\Sigma(\phi)$ mag arcsec^{-2} at an angular distance ϕ'' from the image center. If the coma is in steady-state production (i.e., the surface brightness varies with the inverse of the distance from the nucleus), then $m_c(\phi)$, the total magnitude of the coma inside radius ϕ, is given by Jewitt & Danielson (1984) as

$$m_c(\phi) = \Sigma(\phi) - 2.5 \log\left(2\pi\phi^2\right). \quad (1)$$

From Figure 4, we can be confident that an upper limit to the coma surface brightness at $\phi = 3''$ is $\Sigma(3'') \sim 27$ mag arcsec^{-2}. Substitution into Equation (1) gives $m_c(3.0'') = 22.6$ mag, which is 2.7 mag (factor of $\sim$12) fainter than the total magnitude 19.9 mag in the *R* band. Therefore, we conclude that the magnitude of a coma within a $3''$ radius circle is $\leqslant$0.08 of the measured brightness. This is consistent with, but less stringent than, the limit deduced from the profile-fitting model.

3.3. Size and Active Fractional Area

To derive the size of 2003 EH1, we used results of the *R*-band photometry taken on the nights of UT 2013 August 9 and 12 from KPNO 2.1 (Table 2) and those taken on UT 2013 October 2 from Keck 10 ($R = 20.21 \pm 0.01$ mag and 20.26 ± 0.02 mag). The apparent red magnitude m_R was corrected to the absolute red magnitude, $m_R(1, 1, 0)$ using

$$m_R(1, 1, 0) = m_R - 5 \log(R\, \Delta) - \beta\alpha, \quad (2)$$

where R and Δ are the heliocentric and geocentric distances (both in AU), α (deg) is the phase angle (observer–asteroid–Sun), and β is the linear phase coefficient (mag deg^{-1}). We took $\beta = 0.04$ mag deg^{-1}, which is compatible with values measured for JFC nuclei (Lamy et al. 2004). We used the absolute red magnitude, $m_R(1, 1, 0)$, to calculate the effective object radius in meters, r_e, using Russell (1916)

$$r_e = \frac{1.496 \times 10^8}{\sqrt{p_R}} 10^{0.2(R_\odot - m_R(1,1,0))}, \quad (3)$$

where $R_\odot = -27.1$ is the apparent red magnitude of the Sun (Cox 2000). We adopt the typical value of geometric albedo, $p_v(\approx p_R) = 0.04$, from the visible and thermal (mid-infrared) measurements for JFC nuclei (Lamy et al. 2004; Fernández et al. 2013). For the averaged absolute red magnitude m_R(1, 1,

Table 2
Color Photometry (UT 2013 August 9 and 12)

N	Midtime	$B-R$	$V-R$	$R-I$	$B-V$[a]	R
1	30.87809	⋯	⋯	⋯	⋯	20.21 ± 0.02
2	30.94424	1.10 ± 0.01	⋯	⋯	⋯	20.17[b]
3	31.00062	⋯	0.34 ± 0.02	⋯	0.76 ± 0.02	20.16[b]
4	31.05442	⋯	⋯	⋯	⋯	20.09 ± 0.02
5	31.30880	1.02 ± 0.01	⋯	⋯	⋯	20.13[b]
6	31.36776	⋯	0.45 ± 0.02	⋯	0.57 ± 0.02	20.13[b]
7	31.42471	⋯	⋯	⋯	⋯	20.16 ± 0.02
8	32.73436	⋯	0.31 ± 0.02	⋯	0.71 ± 0.02	20.30[b]
9	32.79421	⋯	⋯	⋯	⋯	20.30 ± 0.02
10	32.95557	1.06 ± 0.01	⋯	⋯	⋯	20.34[b]
11	33.01491	⋯	0.48 ± 0.02	⋯	0.58 ± 0.02	20.35[b]
12	33.07137	⋯	⋯	⋯	⋯	20.36 ± 0.02
13	102.67640	⋯	⋯	⋯	⋯	20.33 ± 0.02
14	102.80208	1.11 ± 0.02	⋯	⋯	⋯	20.40[b]
15	102.86185	⋯	0.39 ± 0.02	⋯	0.72 ± 0.03	20.43[b]
16	102.92412		⋯	⋯	⋯	20.48 ± 0.02
17	103.00632		⋯	0.41 ± 0.04	⋯	20.48[b]
18	103.09013	1.19 ± 0.02	⋯	⋯	⋯	20.51[b]
19	103.15221	⋯	0.42 ± 0.01	⋯	0.77 ± 0.02	20.53[b]
20	103.21338	⋯	⋯	⋯	⋯	20.52 ± 0.02
21	103.29392	⋯	⋯	0.48 ± 0.03	⋯	20.58[b]
22	103.37791	1.02 ± 0.02	⋯	⋯	⋯	20.60[b]
23	103.43949	⋯	0.27 ± 0.02	⋯	0.75 ± 0.03	20.62[b]
24	103.49812	⋯	⋯	⋯	⋯	20.64 ± 0.03
25	103.57827	⋯	⋯	0.37 ± 0.01	⋯	20.65[b]
Average colors[c]	⋯	1.07 ± 0.01	0.39 ± 0.01	0.38 ± 0.01	0.69 ± 0.01	⋯
Solar colors[d]	⋯	0.99 ± 0.02	0.35 ± 0.01	0.33 ± 0.01	0.64 ± 0.02	⋯

Notes.
[a] Calculated from $B-R$ and $V-R$ in this table.
[b] Apparent R-band magnitude interpolated from the light curve data.
[c] The weighted mean of measurements.
[d] Holmberg et al. (2006).

0) = 15.82 ± 0.17 mag, Equation (3) gives $r_e = 1950 \pm 150$ m, which we approximate as $r_e = 2.0 \pm 0.2$ km. The nucleus, represented by a sphere of this radius and assumed bulk density $\rho = 2000$ kg m^{-3} (the density of the Quadrantid meteoroids, Babadzhanov & Kokhirova 2009), is $M_n \sim 6 \times 10^{13}$ kg. This is comparable to, but slightly larger than, the estimated stream mass of (1–2) × 10^{13} kg.

The asteroid 2003 EH1 shows point-like surface brightness. Here we estimate the maximum allowable coma activity. Assuming that water ice still exists and occupies the object surface, we estimate limits to both the ongoing mass loss rate and the fractional active area on the surface. The approximate rate of the isotropic dust ejection from the object is expressed as a function of the parameter η (Luu & Jewitt 1992):

$$\frac{dM}{dt} = \frac{1.0 \times 10^{-3} \pi \rho \bar{a} \eta {r_e}^2}{\theta R^{1/2} \Delta} \tag{4}$$

where $\rho = 2000$ kg m^{-3} is the assumed bulk density determined by the Quadrantid meteoroids (Babadzhanov & Kokhirova 2009), $\bar{a} = 0.5 \times 10^{-6}$ m is the assumed mean grain radius, $r_e = 1950 \pm 150$ m is the effective radius of 2003 EH1, θ is the reference photometry aperture radius of 30 pixels (4″05), and $R = 2.139$ AU, $\Delta = 2.038$ AU given in Table 1. The estimated limit to the mass loss rate is $dM/dt \lesssim 2.5 \times 10^{-2}$ kg s^{-1} with $\eta \lesssim 0.025 \pm 0.007$. The dM/dt is converted into the fraction of active area on the nucleus surface, f_A, using Luu & Jewitt (1992):

$$f_A = \frac{dM/dt}{4\pi r_e^2 \, \mu \, dm/dt}, \tag{5}$$

where dm/dt is the specific sublimation mass loss rate of water in kg m^{-2} s^{-1} and $\mu = 1$ is the assumed dust-to-gas mass ratio (Luu & Jewitt 1992; Greenberg 1998). (A value of $\mu = 4 \pm 2$ was measured in a recent encounter with JFC 67P/Churyumov-Gerasimenko Rotundi et al. 2015.) The dm/dt is calculated from the energy-balance equation

$$\frac{S_\odot(1-A)}{R^2} = \chi\left[\epsilon \sigma T^4 + L(T) dm/dt\right], \tag{6}$$

where $S_\odot = 1365$ W m^{-2} is the solar constant, R (in AU) is the heliocentric distance, $\epsilon = 0.9$ is the wavelength-averaged emissivity, $\sigma = 5.67 \times 10^{-8}$ W m^{-2} K^{-4} is the Stephan–Boltzmann constant and T K is the equilibrium temperature. Quantity A is the Bond albedo, defined by $A = p_v q = 0.012$, where $p_v = 0.04$ (Lamy et al. 2004; Fernández et al. 2013) and $q \sim 0.3$ is the phase integral determined from cometary nuclei and Jupiter Trojan asteroids (Fernández et al. 2003; Buratti et al. 2004). The latent heat of sublimation for water at temperature T (in K) is given by $L(T) = (2.875 \times 10^6) - (1.111 \times 10^3)T$ in J kg^{-1}, taking the polynomial fit to the thermodynamic data in Delsemme & Miller (1971).

Table 3
R-Band Photometry on KPNO 2.1

N	Date (UT 2013)	Midtime[a]	Relative: R[b]
1	Aug 8	4.65021	0.033 ± 0.033
2	Aug 8	4.72038	0.073 ± 0.038
3	Aug 8	4.86321	−0.025 ± 0.045
4	Aug 8	4.95241	−0.059 ± 0.050
5	Aug 8	5.01383	−0.019 ± 0.032
6	Aug 8	5.07517	−0.066 ± 0.036
7	Aug 8	5.13679	−0.014 ± 0.043
8	Aug 8	5.19821	−0.120 ± 0.049
9	Aug 8	5.32672	−0.127 ± 0.035
10	Aug 8	5.51110	−0.087 ± 0.031
11	Aug 8	5.58944	−0.125 ± 0.036
12	Aug 8	5.65078	−0.119 ± 0.033
13	Aug 8	5.71217	−0.087 ± 0.033
14	Aug 8	5.77379	−0.115 ± 0.040
15	Aug 8	5.83524	−0.270 ± 0.038
16	Aug 8	5.93243	−0.245 ± 0.028
17	Aug 8	5.99379	−0.095 ± 0.027
18	Aug 8	6.05513	−0.121 ± 0.027
19	Aug 8	6.11675	−0.073 ± 0.027
20	Aug 8	6.17812	−0.060 ± 0.028
21	Aug 8	6.25545	−0.097 ± 0.036
22	Aug 8	6.31677	−0.172 ± 0.027
23	Aug 8	6.37812	−0.118 ± 0.028
24	Aug 8	6.43947	−0.076 ± 0.032
25	Aug 8	6.50084	−0.105 ± 0.027
26	Aug 8	6.56360	−0.301 ± 0.085
27	Aug 8	6.62498	−0.214 ± 0.081
28	Aug 8	6.68636	−0.057 ± 0.137
29	Aug 8	6.74799	−0.048 ± 0.061
30	Aug 8	6.80937	−0.059 ± 0.053
31	Aug 8	6.88904	−0.278 ± 0.106
32	Aug 8	7.07318	0.137 ± 0.122
33	Aug 8	7.27336	−0.118 ± 0.058
34	Aug 8	7.33471	0.020 ± 0.041
35	Aug 8	7.39608	−0.007 ± 0.034
36	Aug 8	7.45743	−0.139 ± 0.030
37	Aug 8	7.53773	−0.037 ± 0.030
38	Aug 8	7.59908	0.079 ± 0.034
39	Aug 8	7.66049	0.038 ± 0.032
40	Aug 8	7.72209	−0.027 ± 0.035
41	Aug 8	7.78347	0.010 ± 0.031
42	Aug 8	7.85684	0.089 ± 0.037
43	Aug 8	7.91815	0.054 ± 0.031
44	Aug 8	8.10221	0.110 ± 0.033
45	Aug 8	8.18501	0.043 ± 0.035
46	Aug 8	8.24638	0.087 ± 0.035
47	Aug 8	8.30772	0.159 ± 0.031
48	Aug 8	8.36909	0.131 ± 0.031
49	Aug 8	8.43053	0.125 ± 0.035
50	Aug 8	8.50853	0.215 ± 0.033
51	Aug 8	8.56987	0.126 ± 0.030
52	Aug 8	8.63125	0.071 ± 0.032
53	Aug 8	8.69263	0.090 ± 0.030
54	Aug 8	8.75424	0.159 ± 0.036
55	Aug 8	8.82486	0.224 ± 0.039
56	Aug 8	8.88624	0.138 ± 0.032
57	Aug 8	8.94772	0.101 ± 0.038
58	Aug 8	9.00907	0.079 ± 0.036
59	Aug 8	9.07043	0.136 ± 0.035
60	Aug 8	9.14868	0.159 ± 0.034
61	Aug 8	9.21012	0.059 ± 0.038
62	Aug 8	9.27147	0.159 ± 0.034
63	Aug 8	9.33284	0.095 ± 0.034

Table 3
(Continued)

N	Date (UT 2013)	Midtime[a]	Relative: R[b]
64	Aug 8	9.39421	0.108 ± 0.035
65	Aug 8	9.47617	0.103 ± 0.042
66	Aug 8	9.53757	0.008 ± 0.040
67	Aug 8	9.59891	−0.016 ± 0.035
68	Aug 8	9.66027	0.083 ± 0.043
69	Aug 8	9.72165	0.108 ± 0.044
70	Aug 8	9.80528	0.102 ± 0.044
71	Aug 8	9.86663	0.076 ± 0.045
72	Aug 8	9.92799	0.096 ± 0.051
73	Aug 8	9.98936	0.098 ± 0.050
74	Aug 8	10.05075	−0.001 ± 0.042
75	Aug 8	10.15400	0.126 ± 0.045
76	Aug 8	10.21533	0.135 ± 0.057
77	Aug 8	10.33809	0.107 ± 0.055
78	Aug 8	10.39944	−0.056 ± 0.052
79	Aug 8	10.46384	0.023 ± 0.043
80	Aug 8	10.52545	0.030 ± 0.073
81	Aug 8	10.58685	0.091 ± 0.091
82	Aug 8	10.64823	−0.062 ± 0.057
83	Aug 8	10.70965	−0.126 ± 0.055
84	Aug 9	27.81903	0.237 ± 0.049
85	Aug 9	27.88119	0.293 ± 0.049
86	Aug 9	27.96539	0.330 ± 0.060
87	Aug 9	28.02678	0.357 ± 0.063
88	Aug 9	28.08838	0.118 ± 0.052
89	Aug 9	28.14975	0.318 ± 0.067
90	Aug 9	28.21116	0.167 ± 0.053
91	Aug 9	28.42676	0.143 ± 0.036
92	Aug 9	28.48830	0.173 ± 0.033
93	Aug 9	28.54993	0.158 ± 0.034
94	Aug 9	28.61124	0.137 ± 0.034
95	Aug 9	28.67285	0.201 ± 0.033
96	Aug 9	28.75240	0.147 ± 0.033
97	Aug 9	28.81376	0.277 ± 0.037
98	Aug 9	28.87517	0.250 ± 0.041
99	Aug 9	28.93656	0.221 ± 0.038
100	Aug 9	28.99796	0.213 ± 0.038
101	Aug 9	29.06066	0.217 ± 0.035
102	Aug 9	29.12197	0.275 ± 0.036
103	Aug 9	29.30653	0.126 ± 0.034
104	Aug 9	29.37069	0.131 ± 0.038
105	Aug 9	29.43208	0.066 ± 0.030
106	Aug 9	29.49344	0.090 ± 0.029
107	Aug 9	29.55509	0.093 ± 0.031
108	Aug 9	29.61646	0.082 ± 0.031
109	Aug 9	29.67886	0.050 ± 0.026
110	Aug 9	29.74029	0.070 ± 0.026
111	Aug 9	29.80190	0.037 ± 0.025
112	Aug 9	29.86328	−0.043 ± 0.026
113	Aug 9	29.92464	0.034 ± 0.026
114	Aug 9	29.98671	−0.030 ± 0.025
115	Aug 9	30.04833	−0.036 ± 0.023
116	Aug 9	30.10971	−0.137 ± 0.026
117	Aug 9	30.23262	−0.075 ± 0.025
118	Aug 9	30.30721	−0.120 ± 0.026
119	Aug 9	30.36858	−0.075 ± 0.025
120	Aug 9	30.43001	−0.165 ± 0.025
121	Aug 9	30.49167	−0.107 ± 0.028
122	Aug 9	30.55305	−0.100 ± 0.031
123	Aug 9	30.63248	−0.167 ± 0.025
124	Aug 9	30.69387	−0.162 ± 0.024
125	Aug 9	30.75544	−0.136 ± 0.025
126	Aug 9	30.81677	−0.158 ± 0.025

Table 3
(Continued)

N	Date (UT 2013)	Midtime[a]	Relative: R[b]
127	Aug 9	30.87809	−0.151 ± 0.024
128	Aug 9	31.05442	−0.291 ± 0.025
129	Aug 9	31.42471	−0.230 ± 0.026
130	Aug 9	32.79421	−0.061 ± 0.028
131	Aug 9	33.07137	−0.026 ± 0.030
132	Aug 12	99.73628	−0.390 ± 0.050
133	Aug 12	99.79843	−0.332 ± 0.053
134	Aug 12	99.88173	−0.238 ± 0.055
135	Aug 12	99.94330	−0.282 ± 0.052
136	Aug 12	100.00467	−0.270 ± 0.045
137	Aug 12	100.06596	−0.211 ± 0.042
138	Aug 12	100.12734	−0.339 ± 0.048
139	Aug 12	100.33770	−0.225 ± 0.034
140	Aug 12	100.39931	−0.167 ± 0.033
141	Aug 12	100.46064	−0.249 ± 0.043
142	Aug 12	100.52200	−0.250 ± 0.040
143	Aug 12	100.58336	−0.200 ± 0.037
144	Aug 12	100.64521	−0.156 ± 0.039
145	Aug 12	100.70649	−0.392 ± 0.058
146	Aug 12	100.76810	−0.231 ± 0.033
147	Aug 12	100.82973	−0.240 ± 0.031
148	Aug 12	100.89125	−0.218 ± 0.034
149	Aug 12	100.95269	−0.175 ± 0.029
150	Aug 12	101.01404	−0.119 ± 0.036
151	Aug 12	101.07562	−0.122 ± 0.040
152	Aug 12	101.13722	−0.153 ± 0.038
153	Aug 12	101.19859	−0.111 ± 0.032
154	Aug 12	101.26019	−0.172 ± 0.031
155	Aug 12	101.32154	−0.146 ± 0.034
156	Aug 12	101.38279	−0.109 ± 0.038
157	Aug 12	101.44414	−0.170 ± 0.037
158	Aug 12	101.50550	−0.059 ± 0.028
159	Aug 12	101.56772	−0.109 ± 0.025
160	Aug 12	101.62931	−0.048 ± 0.027
161	Aug 12	101.75224	0.013 ± 0.031
162	Aug 12	101.81387	0.008 ± 0.032
163	Aug 12	101.93697	−0.183 ± 0.025
164	Aug 12	101.99857	0.024 ± 0.028
165	Aug 12	102.06017	0.021 ± 0.030
166	Aug 12	102.12178	0.053 ± 0.036
167	Aug 12	102.18341	−0.014 ± 0.034
168	Aug 12	102.24477	−0.196 ± 0.037
169	Aug 12	102.30640	−0.012 ± 0.034
170	Aug 12	102.36801	0.086 ± 0.036
171	Aug 12	102.42936	0.150 ± 0.032
172	Aug 12	102.49235	0.133 ± 0.035
173	Aug 12	102.55367	0.141 ± 0.032
174	Aug 12	102.61504	0.046 ± 0.035
175	Aug 12	102.67640	0.028 ± 0.034
176	Aug 12	102.92412	0.170 ± 0.047
177	Aug 12	103.21338	0.202 ± 0.039
178	Aug 12	103.49812	0.312 ± 0.044
179	Aug 12	104.28804	0.198 ± 0.037
180	Aug 12	104.35062	0.202 ± 0.045
181	Aug 12	104.41201	0.325 ± 0.052
182	Aug 12	104.47354	0.248 ± 0.046
183	Aug 12	104.53492	0.186 ± 0.039
184	Aug 12	104.59631	−0.045 ± 0.034
185	Aug 12	104.65873	0.267 ± 0.044
186	Aug 12	104.72009	0.254 ± 0.045
187	Aug 12	104.90471	0.137 ± 0.036
188	Aug 12	104.99241	0.339 ± 0.076
189	Aug 12	105.05683	0.156 ± 0.047
190	Aug 12	105.11857	0.094 ± 0.073
191	Aug 12	105.18058	0.123 ± 0.039
192	Aug 12	105.30671	0.013 ± 0.065
193	Aug 12	105.36855	0.302 ± 0.062
194	Aug 12	105.42993	0.235 ± 0.045
195	Aug 12	105.49139	0.168 ± 0.036
196	Aug 12	105.67662	0.218 ± 0.050
197	Aug 12	105.73822	0.217 ± 0.051
198	Aug 12	105.79961	0.122 ± 0.054
199	Aug 12	105.86091	−0.106 ± 0.053
200	Aug 12	105.92229	−0.042 ± 0.056
201	Aug 12	105.98367	0.034 ± 0.043
202	Aug 12	106.04529	0.129 ± 0.049
203	Aug 12	106.10664	0.258 ± 0.053
204	Aug 12	106.16805	0.111 ± 0.046
205	Aug 12	106.22961	0.116 ± 0.055

Notes.
[a] Time since UT 2013 August 8.00000. The middle of integration times is taken.
[b] Red magnitude relative to field stars in background.

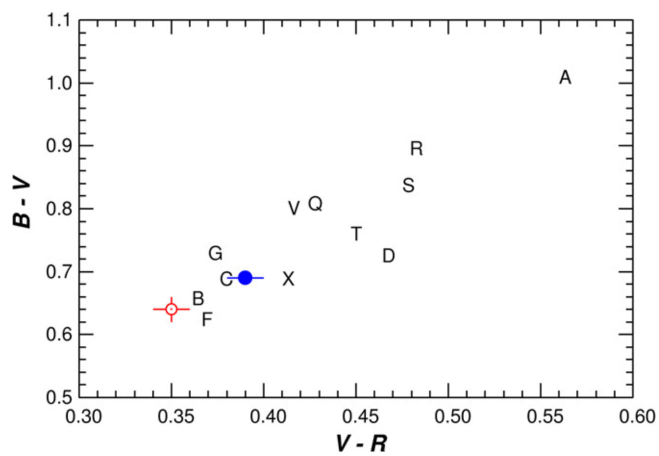

Figure 2. Color plots of $V - R$ vs. $B - V$ for 2003 EH1 (blue circle) on weighted mean and Tholen taxonomic classifications (Tholen 1984), as tabulated by Dandy et al. (2003). The color of the Sun (red circle) is also plotted. The uncertainty of $B - V$ for 2003 EH1 is within the circle.

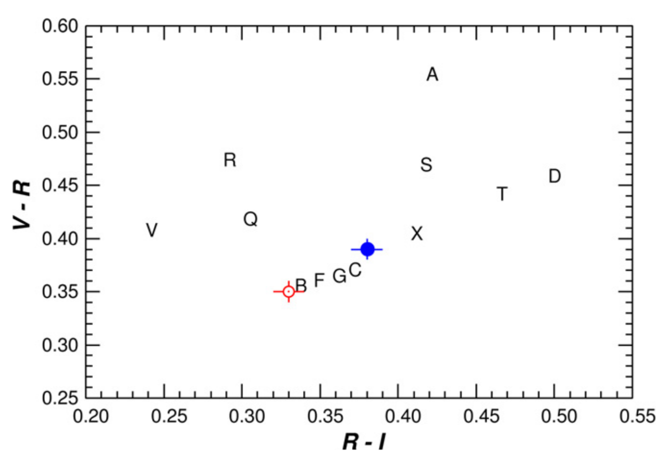

Figure 3. Same as Figure 2 but in the $R - I$ vs. $V - R$ color plane.

Table 4
Measured Colors of 2003 EH1 and Small Body Populations

Object	$V-R$	S'	N[a]	Source
2003 EH1[b]	0.39 ± 0.01	3.7 ± 0.9	…	(1)
KBOs[c]	0.59 ± 0.12	22.0 ± 10.9	297	(2)
Centaurs	0.54 ± 0.01	17.5 ± 0.9	32	(2)
Damocloids[d]	0.48 ± 0.01	12.0 ± 0.9	12	(3)
Nuclei[e]	0.45 ± 0.02	9.2 ± 1.8	12	(4)
Dead comets	0.44 ± 0.02	8.3 ± 1.8	12	(4)
Trojans[f]	0.46 ± 0.01	10.1 ± 0.9	451	(5)
D-types	0.45 ± 0.01	9.2 ± 0.9	19	(6)
MBCs[g]	0.37 ± 0.01	1.8 ± 0.9	6	(7)
Solar color	0.35 ± 0.01	0.0 ± 0.9	…	(8)

Notes. S' from the relation, $V-R = (V-R)_{\odot} + 2.5 \log[(2+S'\Delta\lambda)/(2-S'\Delta\lambda)]$, where $V-R$ and $(V-R)_{\odot} = 0.35$ are the colors of the object and the Sun respectively, and $\Delta\lambda = 1000$ Å is the difference between the V- and R- filters (Luu & Jewitt 1990).
[a] Number of objects in the population.
[b] The weighted mean of measurements from Table 2.
[c] Kuiper Belt Objects.
[d] Inactive cometary nuclei of Halley-family and long-period comets with $T_J \leqslant 2$.
[e] Cometary nuclei.
[f] Jupiter Trojans.
[g] Main belt comets.
References. (1) This work, (2) Peixinho et al. (2015), (Jewitt & Luu 2001 and Bauer et al. 2003 are included), (3) Jewitt (2005), (4) Jewitt (2002), (5) Szabó et al. (2007), (see also Jewitt & Luu 1990 and Karlsson et al. 2009), (6) Fitzsimmons et al. (1994), (7) Hsieh et al. (2004, 2009, 2010, 2011, 2013, 2015), Jewitt et al. (2009), (8) Holmberg et al. (2006).

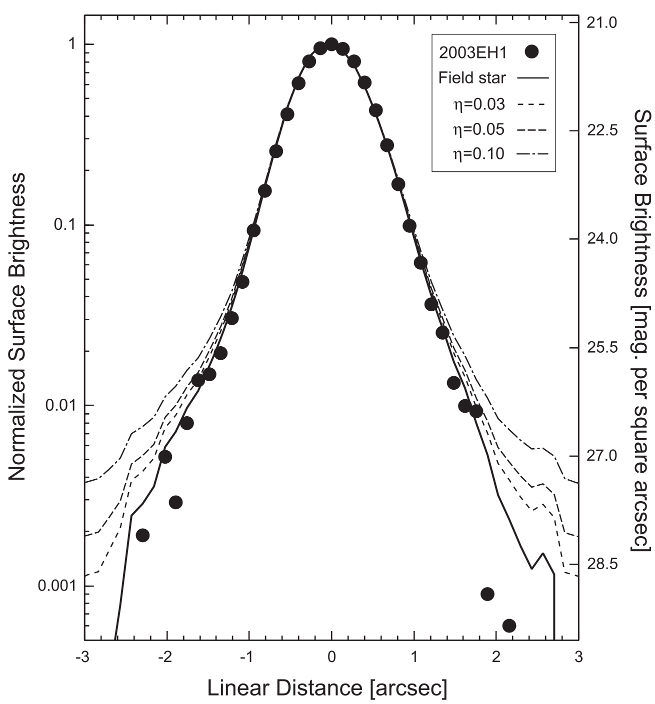

Figure 4. Normalized R-band surface brightness profiles of 2003 EH1, the field star, and seeing-convolution models having coma levels of $\eta = 0.03$, 0.05, and 0.10. One unit of the surface brightness of the asteroid is $\Sigma = 21.3$ mag arcsec^{-2}.

The dimensionless parameter χ represents the ratio of the effective cross-section for emission of thermal radiation from the nucleus to that for absorption of solar power. The lowest value, $\chi = 1$, corresponds to subsolar ice on a non-rotating object, while the highest value, $\chi = 4$, corresponds to an isothermal, spherical nucleus. For comet-like objects, the night-side thermal radiation is negligible (i.e., day-side emission only) due to the low thermal diffusivity of the surface layers, suggesting the intermediate value, $\chi = 2$, is appropriate for providing a maximum active fractional area and minimum specific mass ross rate (Fernández et al. 2013; Li & Jewitt 2015). However, since we are interested in obtaining a limit to f_A, we assume the lowest possible surface temperatures (corresponding to the isothermal case, $\chi = 4$) and find $dm/dt = 7.5 \times 10^{-6}$ kg m^{-2} s^{-1} and $T = 180$ K at $R = 2.139$ AU using Equation (6). To supply 2.5×10^{-2} kg s^{-1} would require an exposed patch of ice on the surface having an area of 3300 m^2, corresponding to $f_A \lesssim 10^{-4}$ according to Equation (5). This fraction is smaller by an order of magnitude than is characteristic of even low activity JFC nuclei (A'Hearn et al. 1995).

3.4. Rotational Period and Shape

To search for the rotation period for 2003 EH1, we used a spectral analysis technique that employs the discrete Fourier transform (DFT) algorithm (Lomb 1976; Scargle 1982) on the relative R-bandtime-series photometric data (Table 3). The DFT analysis evaluates the spectral power as a function of angular frequency using the fitting quality at a given frequency in the data. The maximum power at the frequency indicates the highest significance level, reflecting the most convincing solution for the periodicity. The light curve shape is presumed to be two-peaked as seen in most small bodies in the solar system, implying an elongated body shape. The fitting solution for the two-peaked rotational period is $P_{\rm rot} = 12.650$ hr. The uncertainty on the period is computed using the equation given by Gilliland & Fisher (1985)

$$\frac{\Delta f}{f} = \left[\frac{0.0256}{(fT)^4} + \frac{0.5625\sigma^2}{n(fT)^2 A^2}\right]^{1/2}, \quad (7)$$

where Δf is the root mean square error, f is the number of cycles per day (24 hr), T is the observing period (in days), A is the signal amplitude, n is the number of measurements, and σ^2 is the variance of the data. Substituting $f = 1.8972$ (=24 hr/$P_{\rm rot}$), $T = 4.2299$, $A = 0.44$ mag, $n = 205$, and $\sigma^2 = 0.0025$, we obtain $\Delta f/f \sim 0.26\%$, namely, the uncertainty on the period is ±0.033 hr. The phased light curve with this period, $P_{\rm rot} = 12.650 \pm 0.033$ hr, is shown in Figure 5.

The fitted model for the light curve finds the maximum photometric range of 2003 EH1 is $\Delta m_R = 0.44 \pm 0.01$, which gives a lower limit to the intrinsic axis ratio, a/b, between long axis a and short axis b. Assuming the object's rotational axis is perpendicular to our line of sight, the ratio is expressed as $a/b = 10^{0.4\Delta m_R}$. We find $a/b = 1.50 \pm 0.01$. In practice, this is a lower limit to a/b because the rotation axis may not be perpendicular to the line of sight. Our observations of 2003 EH1 are consistent with the shapes of typical cometary nuclei, which tend to be elongated ($a/b \geqslant 1.5$; Jewitt 2004) relative to asteroids of comparable size. The slow rotation and modest a/b do not present any threat to the rotational stability of 2003 EH1 for bulk densities >100 kg m^{-3}, even assuming zero tensile strength.

Non-central outgassing (mass loss) can generate torques that change the angular momentum of the nucleus and drive an

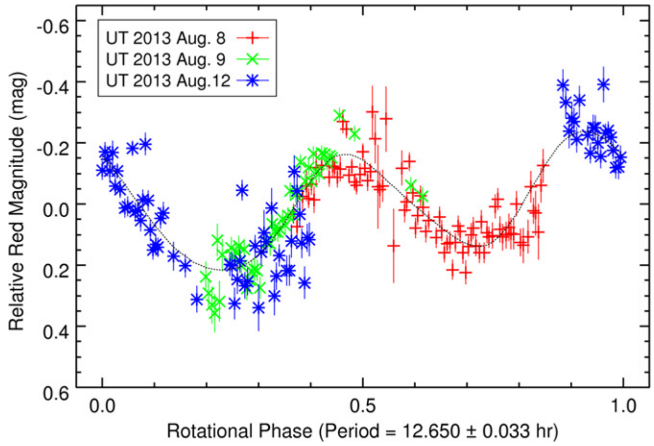

Figure 5. R-band photometry of 2003 EH1 observed on UT 2013 August 8, 9, and 12, phased to the two-peaked period $P_{\rm rot} = 12.650 \pm 0.033$ hr. The dotted curve displays the fitting result having the maximum photometric range $\Delta m_{\rm R} = 0.44 \pm 0.01$ mag.

object into an excited rotational energy state. We estimated the timescale for rotational excitation of 2003 EH1 assuming continuous mass loss at the maximum rate allowed by our data and using the formalism described in Jewitt (1997). With values of the dimensionless moment arm for the torque in the range 10^{-3}–10^{-1}, we obtain excitation timescales in the range from 10^5 to 10^7 year. These are long compared to the few $\times$ 10^4 year active lifetimes of JFC comets (Levison & Duncan 1997), suggesting that rotational excitation of 2003 EH1 is unlikely, at least given the present activity state.

3.5. Mantle Formation

Rubble mantles in comets consist of refractory blocks that are large enough not to be ejected by outgassing drag forces against the gravity of the nucleus, although cohesion also likely plays a role. The timescale for growth of a cohesionless rubble mantle in the presence of a sublimating ice surface is given by Jewitt (2002). From Figure 5 of that paper, we read that the mantling time for a 2 km nucleus between 1 and 5 AU from the Sun is in the range $0.3 \lesssim \tau \lesssim 100$ year. Even the upper limit to the timescale is short compared to the timescale of the dynamical evolution of 2003 EH1, showing that mantle formation is likely and explaining the very low (or absent) present-day mass loss. Given that 2003 EH1 has followed a complicated and rapidly changing dynamical path, including recent close passages by the Sun, it is likely that the existing rubble mantle reflects depletion of near-surface volatiles occurring at higher temperatures than those that now prevail.

The timescale for heat to conduct across the radius of the nucleus, $r_{\rm e}$, is of order $\tau_h \sim r_{\rm e}^2/\kappa$. With $r_{\rm e} = 2$ km and thermal diffusivity $\kappa = 10^{-8}$–10^{-7} m^2 s^{-1} (as appropriate for a porous dielectric material), we find $\tau_h \sim 10^6$–10^7 year. The τ_h exceeds the dynamical lifetime of JFC comets $\tau_{\rm JFC} \sim 10^5$ year (Levison & Duncan 1994) by one or more orders of magnitude, showing that the heat from the Sun would not reach the deep interior of the asteroid during the time spent in the inner solar system. Therefore, we conclude that it is very plausible that 2003 EH1 retains volatiles in its deep interior, but that it is inactive during most of its orbit owing to the recent (and probably recurring) formation of a rubble mantle.

4. DISCUSSION

As noted earlier, the Quadrantid core stream is estimated from dynamical spreading to be 200–500 years in age (Jenniskens 2004; Wiegert & Brown 2005; Abedin et al. 2015). Steady mass loss at the maximum rates allowed by the optical data, namely 2.5×10^{-2} kg s^{-1}, would deliver only about $(1.6–3.9) \times 10^8$ kg in 200–500 years, even if these rates were sustained all around the orbit (which itself seems unlikely). For comparison, the total mass of the meteoroids in the Quadrantid core stream is estimated to be about 10^{13} kg (Jenniskens 2006), which has been updated from earlier estimates of $\leqslant 10^{11-12}$ kg (Hughes & McBride 1989; Jenniskens 1994; Jenniskens et al. 1997). We conclude that the current production rates from 2003 EH1 are about five orders of magnitude too small to supply the mass of the core Quadrantid stream. This result is perhaps not surprising given the current mis-match between the orbits of 2003 EH1 and the Quadrantid stream (Wiegert & Brown 2005).

Could the core stream meteoroids have been released from 2003 EH1 a few centuries ago, when the perihelion was substantially smaller? For example, 200–500 years ago, the perihelion distance was $\sim$0.7–0.9 AU (Jenniskens 2004; Wiegert & Brown 2005). We solved Equation (6) to find hemispherically averaged specific mass loss rates $(2.8–4.9) \times 10^{-4}$ kg m^{-2} s^{-1} at these distances, only 2–3 times larger than at 1.2 AU. Thus, perihelion variations alone are not sufficient to account for the mass of the Quadrantids. Within the context of the equilibrium sublimation model, only by changing the active fraction, f, can the production rates and the stream mass be reconciled. For example, setting $dm/dt = 4.9 \times 10^{-4}$ kg m^{-2} s^{-1} and $f_A = 1$ in Equation (5), we find that the stream mass could be supplied by equilibrium sublimation in $\sim$30 years. We consider it more likely that the injection of mass to the meteoroid stream occurred out of equilibrium, perhaps by a volatile-driven process related to cometary outbursts or break-ups, and triggered by deep penetration of conducted heat into the ice-rich interior of this body.

Intense solar heating can cause fracturing and dust production through thermal fracture and desiccation. For example, asteroid (3200) Phaethon, the parent body of the Geminid meteoroid stream, has shown recurrent activity around its perihelion $q \sim 0.14$ AU (Jewitt & Li 2010; Jewitt et al. 2013; Li & Jewitt 2013) where the surface temperature reaches 750 K $\leqslant T \leqslant$ 1100 K (Ohtsuka et al. 2009). Phaethon is essentially a "rock comet" and the activity is caused by the production of small dust particles with radii $\sim 1\,\mu$m due to thermal fracture and decomposition cracking of hydrated minerals (not sublimation of ice). Since 2003 EH1 recently possessed similarly small perihelia (Neslušan et al. 2013a; Fernández et al. 2014), thermal fracture and surface desiccation may likewise be expected. At its smallest perihelion, $q \sim 0.12$ AU, we estimate surface temperatures of 800 K $\leqslant T \leqslant$ 1200 K on 2003 EH1. However, as on (3200) Phaethon, the particles produced this way should be of micron size and swept from the nucleus by solar radiation pressure (Jewitt et al. 2013, 2015), so that they do not contribute to the meteoroid streams of either body.

Spectroscopic measurements of the Na contents in the meteoroid streams are also suggestive of thermal processing of the parent bodies. The Geminid meteoroids show extreme diversity in their Na abundance, from strong depletion to near

Sun-like Na content (Harvey 1973; Borovička et al. 2005; Kasuga et al. 2005). Presumably, this compositional diversity reflects different thermal modification on Phaethon (or perhaps the larger sized precursor body) itself (Jewitt & Hsieh 2006; Kasuga et al. 2006; Ohtsuka et al. 2006; Kasuga & Jewitt 2008; Ohtsuka et al. 2008; Capek & Borovička 2009; Kasuga 2009; Ohtsuka et al. 2009). For the Quadrantid meteoroids, the measured line intensity ratios show that Na is less depleted than in the majority of Geminid meteoroids (Koten et al. 2006; Borovička et al. 2010). This may imply less thermal modification on 2003 EH1 even though it recently had perihelion distances smaller than Phaethon's. Alternatively, the Quadrantid meteoroids could be released from sub-surface regions on 2003 EH1 deeper than a thermal skin depth and thereby have escaped the most severe thermal effects (Koten et al. 2006).

5. SUMMARY

Optical observations of suggested Quadrantid stream parent 2003 EH1 lead to the following results.

1. The absolute red magnitude, $m_R(1, 1, 0) = 15.82 \pm 0.17$ mag, corresponds to an effective radius $r_e = 2.0 \pm 0.2$ km assuming a red geometric albedo $p_R = 0.04$. The ratio of the nucleus mass to the Quadrantid stream mass is $\sim$3–6, although uncertainty remains because both masses are approximate.
2. The surface brightness profile is point-like, limiting the fractional light scattered by steady-state, near-nucleus coma to $\leqslant$2.5%. The maximum mass loss rate deduced from a model fitted to the profile is $\sim 2.5 \times 10^{-2}$ kg s^{-1}. Water ice can occupy a fraction of the surface no larger than $f_A < 10^{-4}$.
3. The two-peaked rotational light curve has a period $P_{\rm rot} = 12.650 \pm 0.033$ hr. The photometric range, $\Delta m_R = 0.44 \pm 0.01$, indicates a minimum axis ratio of 1.50 ± 0.01.
4. The optical colors ($B - V = 0.69 \pm 0.01$, $V - R = 0.39 \pm 0.01$, and $R - I = 0.38 \pm 0.01$) are slightly redder than the Sun and consistent with the mean colors of dead or dormant cometary nuclei.
5. Current dust production from 2003 EH1 is orders of magnitude too small to supply the mass of the Quadrantid core meteoroid stream in the 200–500 year dynamical lifetime. If 2003 EH1 is the source of the Quadrantids, we infer that mass must be delivered episodically, not in steady-state.

We acknowledge Lusine Kamikyan for assistance with the observations at the KPNO 2.1 telescope. T.K. is grateful for support for this work provided by Tomoko Arai and Takafumi Matsui, in collaboration with the International Space Station METEOR project at the Planetary Exploration Research Center, Chiba Institute of Technology. T.K. is also grateful for financial support from the National Astronomical Observatory of Japan and a Young Researcher Overseas Visit Program (2013), The Graduate University for Advanced Studies. D.J. appreciates support of this work from NASA's Solar System observations program. We thank Dianne Harmer, Beatrice Mueller, Anna Daniel, and other members of the KPNO 2.1 telescope team for their help in planning and scheduling the observations. We thank Joel Aycock for operating the Keck telescope and the anonymous referee for comments. Some of the data presented herein were obtained at the W. M. Keck Observatory, which is operated as a scientific partnership among the California Institute of Technology, the University of California, and the National Aeronautics and Space Administration. The Observatory was made possible by the generous financial support of the W. M. Keck Foundation.

REFERENCES

Abedin, A., Spurný, P., Wiegert, P., et al. 2015, Icar, 261, 100
A'Hearn, M. F., Millis, R. L., Schleicher, D. G., Osip, D. J., & Birch, P. V. 1995, Icar, 118, 223
Babadzhanov, P. B., & Kokhirova, G. I. 2009, A&A, 495, 353
Babadzhanov, P. B., & Obrubov, Y. V. 1991, LPICo, 765, 8
Babadzhanov, P. B., Williams, I. P., & Kokhirova, G. I. 2008, MNRAS, 386, 2271
Bauer, J., Meech, K., Fernández, Y., et al. 2003, Icar, 166, 195
Borovička, J., Koten, P., Spurný, P., Boček, J., & Štork, R. 2005, Icar, 174, 15
Borovička, J., Koten, P., Spurný, P., et al. 2010, IAU Symp. 263, ICY Bodies of the Solar System (Cambridge: Cambridge Univ. Press), 218
Buratti, B. J., Hicks, M. D., Soderblom, L. A., et al. 2004, Icar, 167, 16
Capek, D., & Borovička, J. 2009, Icar, 202, 361
Cox, A. N. 2000, Allen's Astrophysical Quantities (New York: Springer)
Dandy, C. L., Fitzsimmons, A., & Collander Brown, S. J. 2003, Icar, 163, 363
Delsemme, A. H., & Miller, D. C. 1971, P&SS, 19, 1229
Fernández, J. A., Sosa, A., Gallardo, T., & Gutiérrez, J. N. 2014, Icar, 238, 1
Fernández, Y. R., Kelley, M. S., Lamy, P. L., et al. 2013, Icar, 226, 1138
Fernández, Y. R., Sheppard, S. S., & Jewitt, D. C. 2003, AJ, 126, 1563
Fitzsimmons, A., Dahlgren, M., Lagerkvist, C., Magnusson, P., & Williams, I. 1994, A&A, 282, 634
Fornasier, S., Dotto, E., Hainaut, O., et al. 2007, Icar, 190, 622
Gilliland, R. L., & Fisher, R. 1985, PASP, 97, 285
Gonczi, R., Rickman, H., & Froeschle, C. 1992, MNRAS, 254, 627
Greenberg, J. M. 1998, A&A, 330, 375
Harvey, G. A. 1973, NASA SP, 319, 103
Holmberg, J., Flynn, C., & Portinari, L. 2006, MNRAS, 367, 449
Hsieh, H. H., Hainaut, O., Novaković, B., et al. 2015, ApJL, 800, L16
Hsieh, H. H., Ishiguro, M., Pedro Lacerda, P., & Jewitt, D. 2011, AJ, 142, 29
Hsieh, H. H., & Jewitt, D. 2006, Sci, 312, 561
Hsieh, H. H., Jewitt, D., Lacerda, P., Lowry, S. C., & Snodgrass, C. 2010, MNRAS, 403, 363
Hsieh, H. H., Jewitt, D. C., & Fernández, Y. R. 2004, AJ, 127, 2997
Hsieh, H. H., Jewitt, D. C., & Ishiguro, M. 2009, AJ, 137, 157
Hsieh, H. H., Kaluna, H. M., Novaković, B., et al. 2013, ApJL, 771, L1
Hughes, D. W., & McBride, N. 1989, MNRAS, 240, 73
Jenniskens, P. 1994, A&A, 287, 990
Jenniskens, P. 2004, AJ, 127, 3018
Jenniskens, P. 2006, Meteor Showers and Their Parent Comets (Cambridge: Cambridge Univ. Press)
Jenniskens, P., Betlem, H., de Lignie, M., Langbroek, M., & van Vliet, M. 1997, A&A, 327, 1242
Jewitt, D. 1997, EM&P, 79, 35
Jewitt, D. 2005, AJ, 129, 530
Jewitt, D. 2013, AJ, 145, 133
Jewitt, D., & Danielson, G. E. 1984, Icar, 60, 435
Jewitt, D., & Hsieh, H. H. 2006, AJ, 132, 1624
Jewitt, D., Hsieh, H. H., & Agarwal, J. 2015, in Asteroids IV, ed. P. Michel, F. DeMeo & W. Bottke (Tucson, AZ: Univ. Arizona Press), in press
Jewitt, D., & Li, J. 2010, AJ, 140, 1519
Jewitt, D., Li, J., & Agarwal, J. 2013, ApJL, 771, L36
Jewitt, D., & Luu, J. 2001, AJ, 122, 2099
Jewitt, D., Yang, B., & Haghighipour, N. 2009, AJ, 137, 4313
Jewitt, D. C. 2002, AJ, 123, 1039
Jewitt, D. C. 2004, in Comets II, Vol. 745, ed. M. C. Festou, H. U. Keller & H. A. Weaver (Tucson, AZ: Univ. of Arizona Press), 659
Jewitt, D. C., & Luu, J. X. 1990, AJ, 100, 933
Jones, J., & Jones, W. 1993, MNRAS, 261, 605
Jopek, T. J. 2011, MmSAI, 82, 310
Kanuchová, Z., & Neslušan, L. 2007, A&A, 470, 1123
Karlsson, O., Lagerkvist, C.-I., & Davidsson, B. 2009, Icar, 199, 106
Kasuga, T. 2009, EM&P, 105, 321
Kasuga, T., & Jewitt, D. 2008, AJ, 136, 881
Kasuga, T., Watanabe, J., & Ebizuka, N. 2005, A&A, 438, L17

Kasuga, T., Yamamoto, T., Kimura, H., & Watanabe, J. 2006, A&A, 453, L17
Koten, P., Borovička, J., Spurný, P., et al. 2006, MNRAS, 366, 1367
Lamy, P. L., Toth, I., Fernandez, Y. R., & Weaver, H. A. 2004, in Comets II, Vol. 745, ed. M. C. Festou, H. U. Keller & H. A. Weaver (Tucson, AZ: Univ. of Arizona Press), 223
Landolt, A. U. 1992, AJ, 104, 340
Levison, H. F., & Duncan, M. J. 1994, Icar, 108, 18
Levison, H. F., & Duncan, M. J. 1997, Icar, 127, 13
Li, J., & Jewitt, D. 2013, AJ, 145, 154
Li, J., & Jewitt, D. 2015, AJ, 149, 133
Licandro, J., Tancredi, G., Lindgren, M., Rickman, H., & Hutton, R. G. 2000, Icar, 147, 161
Lomb, N. R. 1976, ApJS, 39, 447
Luu, J. X., & Jewitt, D. C. 1990, AJ, 100, 913
Luu, J. X., & Jewitt, D. C. 1992, Icar, 97, 276
McIntosh, B. A. 1990, Icar, 86, 299
Meech, K. J., Hainaut, O. R., & Marsden, B. G. 2004, Icar, 170, 463
Neslušan, L., Hajduková, M., & Jakubík, M. 2013a, A&A, 560, A47
Neslušan, L., Kanuchová, Z., & Tomko, D. 2013b, A&A, 551, A87
Neslušan, L., Kanuchová, Z., & Tomko, D. 2014, in Proc. Astronomical Conf. 2013, Meteoroids, ed. T. J. Jopek et al. (Poznań: Adam Mickiewicz Univ. Press), 235
Ohtsuka, K., Ito, T., Arakida, H., & Yoshikawa, M. 2008, M&PSA, 43, 5055
Ohtsuka, K., Nakato, A., Nakamura, T., et al. 2009, PASJ, 61, 1375
Ohtsuka, K., Sekiguchi, T., Kinoshita, D., et al. 2006, A&A, 450, L25
Ohtsuka, K., Yoshikawa, M., & Watanabe, J. 1995, PASJ, 47, 477
Ohtsuka, K., Yoshikawa, M., Watanabe, J., et al. 2008, EM&P, 102, 179
Oke, J. B., Cohen, J. G., Carr, M., et al. 1995, PASP, 107, 375
Peixinho, N., Delsanti, A., & Doressoundiram, A. 2015, A&A, 577, A35
Quetelet, A. 1839, Nouveaux Memoires de l'Academie Royale des Sciences et Belles and Letters de Bruxelles, 12, 1
Rockosi, C., Stover, R., Kibrick, R., et al. 2010, Proc. SPIE, 7735, 77350R
Rotundi, A., Sierks, H., Della, C. V., et al. 2015, Sci, 347, aaa3905
Russell, H. N. 1916, ApJ, 43, 173
Scargle, J. D. 1982, ApJ, 263, 835
Sekanina, Z., & Chodas, P. W. 2005, ApJS, 161, 551
Skiff, B. A. 2003, Minor Planet e-Circ, 2003-E27, http://www.minorplanetcenter.net/mpec/K03/K03E27.html
Szabó, Gy. M., Ivezic, Z., Juric, M., & Lupton, R. 2007, MNRAS, 377, 1393
Tancredi, G. 2014, Icar, 234, 66
Tholen, D. J. 1984, PhD thesis, Univ. Arizona
Wiegert, P. A., & Brown, P. 2005, Icar, 179, 139
Williams, I. P., Ryabova, G. O., Baturin, A. P., & Chernitsov, A. M. 2004, MNRAS, 355, 1171